



**The effect of chemically preintercalated alkali ion on
structure of layered titanates and their electrochemistry in
aqueous energy storage systems**

Journal:	<i>Journal of Materials Chemistry A</i>
Manuscript ID	TA-ART-04-2020-004545.R1
Article Type:	Paper
Date Submitted by the Author:	16-Jul-2020
Complete List of Authors:	Mukherjee, Santanu; Drexel University, Materials Science and Engineering Quilty, Calvin; Stony Brook University Yao, Shanshan; Brookhaven National Laboratory Stackhouse, Chavis; Stony Brook University Wang, Lei; Brookhaven National Laboratory Takeuchi, Kenneth; Stony Brook University, Chemistry Takeuchi, Esther; Stony Brook University, Materials Science and Engineering Wang, Feng; Brookhaven National Laboratory, Marschilok, Amy; Stony Brook University, Materials Science and Engineering Pomerantseva, Ekaterina; Drexel University, Materials Science and Engineering; Drexel University

The effect of chemically preintercalated alkali ion on structure of layered titanates and their electrochemistry in aqueous energy storage systems

Santanu Mukherjee^a, Calvin D. Quilty^b, Shanshan Yao^c, Chavis A. Stackhouse^b, Lei Wang^c, Kenneth J. Takeuchi^{c,d}, Esther S. Takeuchi^{b,c,d}, Feng Wang^c, Amy C. Marschilok^{b,c,d}, Ekaterina Pomerantseva^{a*}

^a Department of Materials Science and Engineering, Drexel University, Philadelphia, PA, USA, 19104

^b Department of Chemistry, Stony Brook University, Stony Brook, NY, USA, 11794

^c Energy and Photon Sciences Directorate, Brookhaven National Laboratory, Upton, NY, USA, 11973

^d Department of Materials Science and Chemical Engineering, Stony Brook University, Stony Brook, NY, USA, 11794

*Corresponding Author

E-mail: ep423@drexel.edu

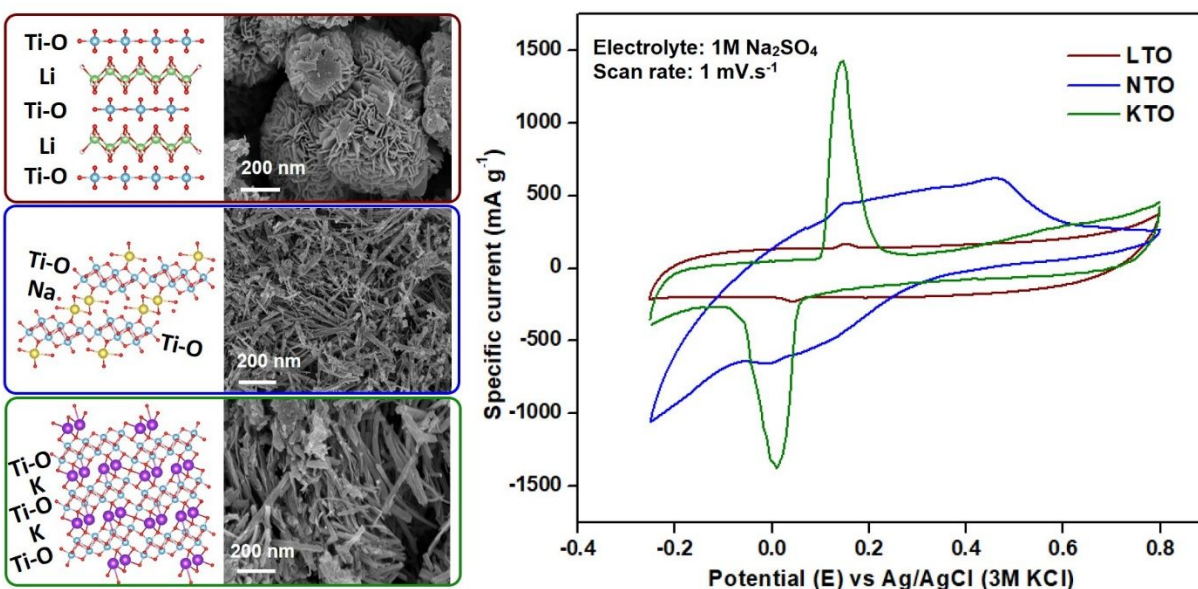
Abstract

We introduce a novel chemical preintercalation based synthesis technique based on hydrogen peroxide induced sol-gel process to obtain alkali ion containing ternary layered titanates (MTO, where M = Li, Na, K). Synthesis parameters leading to the formation of single-phase materials with homogeneous elemental distribution are reported for each of the preintercalated ion. Our analyses indicate that the interlayer spacing in the structure of the layered titanates increases with the increase of the radius of the hydrated preintercalated ion. Scanning and transmission electron microscopy imaging revealed morphological diversity: the LTO phase crystallized as nanoplates assembled in “peony-like” spherical agglomerates while NTO and KTO particles exhibited one-dimensional nanobelt or wire-like morphology, with the KTO nanobelts being shorter and more aggregated than the NTO nanobelts. Structural refinement corroborated by electron diffraction and high-resolution transmission electron microscopy revealed that the structure of the LTO phase is built by stacking Ti-O layers containing a single straight layer of connected TiO₆ octahedra. The layers in NTO and KTO structures form differently and consist of double Ti-O layers with ragged arrangement of units built by TiO₆ octahedra with two titanium rows. The NTO electrodes exhibited the highest electrochemical performance in cells with aqueous

1 M Na₂SO₄ electrolyte, followed by the KTO electrodes and then LTO electrodes, and this trend is maintained at various scan rates. The established relationships between the structure and electrochemical performance reveal that, in addition to interlayer distance and chemistry of the interlayer region, the structure of the layers can play an important role in charge storage properties of layered oxide electrodes. The double Ti-O layers in the structure of NTO and KTO phases provide a larger number of redox centers which could contribute to the superior electrochemical performance as compared to the LTO electrodes. Our findings indicate that layered materials containing double transition metal oxide layers are promising candidates for exfoliation and assembly with electronically conductive layers with the aim to create 2D heterostructures with high electrochemical performance.

Keywords: sol-gel process; chemical preintercalation; layered titanium oxides; aqueous energy storage systems

Graphical Abstract



1. Introduction

With the current focus on transitioning towards renewable and cleaner sources of energy generation, such as solar, wind and hydroelectric, so as to reduce the global carbon footprint and achieve the ambitious “net-zero” emission goal by 2050, due to their intermittent nature it is imperative to develop safe, economically viable, robust and reliable energy storage systems¹⁻². Toward this objective, high-performing, environmentally friendly, affordable, stable and scalable synthesis procedures and materials systems with the ability to perform reliably in aqueous electrolyte systems need to be developed³⁻⁶.

Titanium based oxides are earth-abundant, economically feasible and non-toxic materials that are stable in water, and thus they address many of the challenges posed in this search for novel material systems for advanced electrochemical energy storage⁷⁻⁸. It is expected that in intercalation-based energy storage, the $\text{Ti}^{4+}/\text{Ti}^{3+}$ redox couple will be accessible which will enable significant redox activity. However, there are several challenges that still need to be overcome to realize the full potential of titanium oxides for electrochemical energy storage applications. For example, the three most thermodynamically stable titanium oxide phases, *i.e.* anatase, rutile and brookite, exist as three-dimensional densely packed structures and do not present well defined channels for the diffusion of ions⁹. As a result of dense packing of atoms, their electrochemical activity is limited to surface based reactions, leading to unimpressive performance¹⁰.

Therefore, it is essential to develop novel materials systems coupled with scalable yet facile synthesis techniques, such that both electrochemical activity and charge storage capacities are enhanced, along with improved kinetics. An important way in which all these aspects can be achieved together is by designing electrodes such that they offer pathways for more efficient intercalation-based storage phenomena. Among the novel materials being considered, layered materials have received considerable research interest, due to the presence of two-dimensional structural channels available for reversible intercalation of electrochemically cycled ions¹¹⁻¹². Alkali ion preintercalated oxides of titanium (titanates), existing solely as A-Ti-O (A = Li, Na, K) ternary alkali titanates and presenting lamellar ordering of the structural layers, have therefore, drawn considerable attention as electrode materials for energy storage¹³⁻¹⁴. The structural Ti-O layers are built by TiO_6 octahedra that share corners and/or edges, while the interlayer region is occupied by alkali metal ions, protons and water molecules¹⁵⁻¹⁶. Due to the multiple possibilities of connecting TiO_6 octahedra, the structure of Ti-O layers can vary substantially. However, the

details of structural arrangement of Ti and O atoms in layers cannot be easily understood from the analysis of XRD patterns since the latter are dominated by reflections corresponding to the lamellar stacking of the layers. Therefore, some inconsistencies exist in literature with respect to the structure of layered titanates.

The structural versatility of layered ternary alkali titanates can be clearly seen in the Na-Ti-O system. The general formula describing phases forming in this system can be written as $\text{Na}_2\text{O} \cdot n\text{TiO}_2$. The material composition and structure depend on the value of n : $\text{Na}_2\text{Ti}_3\text{O}_7$ ($n = 3$), $\text{Na}_2\text{Ti}_6\text{O}_{13}$ ($n = 6$), $\text{Na}_2\text{Ti}_7\text{O}_{15}$ ($n = 7$) and $\text{Na}_2\text{Ti}_9\text{O}_{19}$ ($n = 9$)^{15, 17}. Based on the number of Ti atoms in unit formula, the latter material is called sodium nonatitanate, and this is the most widely studied layered ternary alkali titanate for energy storage applications.

The first report for the synthesis of sodium nonatitanate was by Watanabe *et al.*, who synthesized it by a hydrothermal procedure using amorphous TiO_2 and aqueous NaOH solution as precursors¹⁸. While understanding of correlations between XRD patterns and structure of layered titanates, especially for Li- and K-containing phases, is lacking, Sasaki *et al.* have determined that the sodium containing system demonstrates a *P*-type orthorhombic structure¹⁹. It has also been observed that the time of hydrothermal treatment strongly affects the final morphology and structure of the materials. Huang *et al.* have demonstrated that when TiO_2 was hydrothermally treated in NaOH for different time periods, nanotubes were obtained at around 12 hours of hydrothermal treatment, which converted to nanowires when hydrothermal treatment was extended beyond 40 hours²⁰. Structural characterization has shown that the nanowires crystallized in $\text{NaTi}_2\text{O}_4(\text{OH})$ phase, whereas nanotubes corresponded to $\text{NaTi}_2\text{O}_5 \cdot \text{H}_2\text{O}$ phase²⁰.

Therefore, it is these favorable structural aspects of the layered titanates i.e. diversity of phases with tunable morphology, interlayer spacing and hydration content and open channels facilitating ion diffusion contributing to greater electrochemical activity, that have made them attractive as electrode materials for lithium (LIB) and sodium-ion batteries (SIB)²¹⁻²². Pioneering work involving the application of sodium nonatitanates in battery systems have been performed by Shirpour *et al.*^{15-16, 23}. They demonstrated a specific capacity of 125 mAh g^{-1} in non-aqueous LIB system, with interstitial water hindering the ability to obtain good reversibility and stable cycling¹⁵. Performance degradation was ascribed to electrochemical and chemical processes in the cell associated with free water that may have deintercalated from the electrode structure during cycling. Such degradation mechanisms, however, can be mitigated when aqueous systems are

used. Fleischmann *et al.* synthesized a family of layered hydrogen titanates, among which $\text{H}_2\text{Ti}_3\text{O}_7$ delivered a maximum capacity of 80 mAh g^{-1} at a scan rate of 10 mV s^{-1} in $1 \text{ M H}_2\text{SO}_4$ solution²⁴. The superior capacity value was attributed to structural protonation which reduced the structural strain during reversible proton intercalation processes²⁴. However, there is no comprehensive body of work that has studied the performance of layered titanates as electrode materials in neutral aqueous electrolytes with charge carrying ions larger than protons.

Many existing reports show only a single layered titanate phase or a few materials. No systematic studies of a series of samples, from which correlations could be derived, exist. In this work, the synthesis, structure and electrochemical properties of layered $\text{M}_x\text{TiO}_{2\pm z}\cdot n\text{H}_2\text{O}$ ($\text{M} = \text{Li}, \text{Na}, \text{K}$) titanates are characterized carefully. Based on the nature of interlayer ion, we call synthesized materials LTO ($\text{Li}_x\text{TiO}_{2\pm z}\cdot n\text{H}_2\text{O}$), NTO ($\text{Na}_x\text{TiO}_{2\pm z}\cdot n\text{H}_2\text{O}$) and KTO ($\text{K}_x\text{TiO}_{2\pm z}\cdot n\text{H}_2\text{O}$). We show the influence of the facile sol-gel process-based synthesis conditions on the morphology, structure and electrochemical performance of layered titanates in a neutral aqueous electrolyte. Our results indicate that the structure of the Ti-O layers can be a factor in redox activity of layered electrode materials.

2. Experimental processes and techniques

2.1 Materials synthesis

The inorganic alkali ion pre-intercalated layered titanates have been synthesized using an aqueous sol-gel route, modified from previous reports²⁵⁻²⁷. Empirically, the sol-gel process involves the dissolution of metallic Ti in a strong basic solution by addition of hydrogen peroxide to form an intermediate peroxy-titanate complex consisting of $\text{TiO}_4(\text{OH})_2$ octahedra as the building blocks. The rearrangement and intergrowth of building blocks starts the process of the formation of the layered structure with alkali metal ions from the basic precursor being trapped in the interlayer region. Further hydrothermal treatment of the aged precipitate converts the structure of the material to a more uniform layered phase, with the preintercalated alkali ions residing between the layers. Therefore, the role of these preintercalated ions is to guide and preserve the lamellar stacking of Ti-O layers by acting as “pillars”. A schematic illustration and characteristic photographs of the synthesis process consisting in a sol-gel step, followed by extended aging²⁶ and hydrothermal treatment is shown in **Figure 1**. Concentrations of the MOH ($\text{M} = \text{Li}, \text{Na}, \text{K}$) base solution in which Ti was dissolved (X) and during hydrothermal treatment (Y), volume of 30 wt.

% solution of hydrogen peroxide (V) and temperature of the hydrothermal treatment (T) were optimized individually for each alkali ion studied in this work to produce single phase layered titanates (**Table 1**).

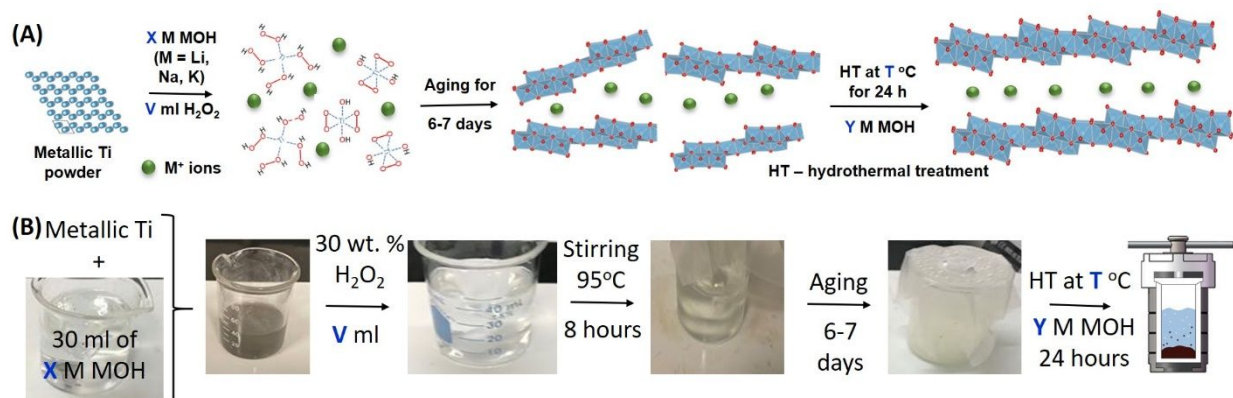


Figure 1. Synthesis process for the preparation of layered titanates stabilized by alkali (Li^+ , Na^+ and K^+) ions. (a) Schematic illustration of the process. (b) Photographs of the materials at various stages of the synthesis. The metallic Ti powder is dissolved in basic aqueous solution *via* addition of H_2O_2 . On subsequent aging for a week, short range order develops in the structure (proto-layering) which converts to a more ordered and layered morphology during hydrothermal treatment²⁸. The parameters shown in blue are alkali ion specific and the values leading to the single-phase formation are shown in Table 1.

Table 1. Concentrations of the MOH (M = Li, Na, K) base solution in which Ti was dissolved (X) and during hydrothermal treatment (Y), volume of 30 wt. % solution of hydrogen peroxide (V) and temperature of the hydrothermal treatment (T) leading to the formation of single phase LTO, NTO and KTO layered titanates.

Alkali metal, M	X (M)	V (ml)	Y (M)	T (°C)
Li	1	15	1	150
Na	10	2	3	220
K	10	5	3	220

Experimentally, the optimization of the synthesis parameters was critical, as the sol-gel process proceeds differently for the three materials, dictated by the thermodynamics and kinetics of the reaction system. Detailed discussion of the optimization of the synthesis parameters for each system is provided in the Supporting Information. The final optimized synthesis conditions established in this work are provided below.

For the synthesis of NTO and KTO phases, 2 ml of 30 wt. % H_2O_2 was added to 30 ml of 10 M MOH (M = Na, K). This was followed by the addition of 0.2 g of Ti powder (Sigma, 98 %)

and the subsequent raising of the temperature up to 95 °C under stirring. The Na-containing solution formed a greyish-white precipitate almost instantly. In case of the K-containing solution, to ensure the complete dissolution of all Ti powder, an excess 3 ml of 30 wt. % H₂O₂ was further added dropwise. In the case of the Na-containing system, the color of the precipitate turned from pale grey to white rapidly (~ 2 h), whereas the K-containing solution turned completely transparent after about 2 hours of the excess of hydrogen peroxide addition. The Na- and K-containing solutions were stirred at 95 °C for 8 hours and then aged for a week at room temperature to allow for the layered phases to form²⁶. No notable changes were observed in appearance of the white precipitate in case of Na-containing system over the course of aging. However, in case of the K-containing solution, small flaky needle-like white particles precipitated from approximately the fourth day onwards. The step-by-step photographs of the color change and precipitate formation for the NTO and KTO samples are shown in **Figure S1(a-c)** and **Figure S2(a-e)** in the Supporting Information. The role of aging is important as it strongly influences the development of the lamellar ordering and as shown in **Figure S3** of the Supporting Information. Aging for a week was followed by hydrothermal treatment in the corresponding base solutions.

For the synthesis of LTO, the initial starting solution consisted of 20 ml of 1 M LiOH and 15 ml of 30 wt. % H₂O₂. To this solution, 0.2 g of Ti powder (Sigma, 98 %) was added and allowed to stir steadily at a temperature of 95 °C for 8 hours. The initially formed dark-colored suspension of metallic titanium powder lightened with time until a white precipitate formed after 2 hours. After 8 hours, the heat and stirring were both discontinued and the solution was aged for a week under ambient conditions. It has been observed that starting with 10 M LiOH and 5 ml H₂O₂ does not result in complete dissolution of the metallic Ti. A substantially diluted initial basic solution, 1 M LiOH, and 15 ml of 30 wt. % H₂O₂ were found to be the appropriate conditions for the complete dissolution of titanium powder as shown in **Figure S4** (Supporting Information). The precipitate was dispersed in 1 M LiOH in a Teflon lined autoclave (Parr Instrument) and hydrothermally treated at 150 °C for 24 hours. For the synthesis of NTO and KTO, the precipitates were dispersed in 3 M NaOH/KOH solution, respectively, followed by hydrothermal treatment at 220 °C for 24 hours. The solid products of hydrothermal treatment were collected by vacuum filtration with thorough washing and subsequently dried in air at 105 °C overnight. It is to be noted that in case of Li-containing system, using high temperature of hydrothermal treatment (220 °C) resulted in the formation of anatase phase instead of layered titanate structure, whereas the higher

temperatures (220 °C) helped the formation of the NTO and KTO phases, as shown in **Figure S5** in the Supporting Information. On the other hand, the usage of low temperature (150°C) and/or shorter hydrothermal treatment times for the preparation of NTO and KTO phases, to mimic the LTO synthesis conditions, did not result in a good phase formation, as observed from the XRD patterns in **Figure S6(a, b)** in the Supporting Information.

2.2 Materials characterization

A Rigaku SmartLab X-ray diffractometer with Cu K α radiation was utilized to analyze the phase composition of the materials. XRD patterns were acquired in the 2θ range of 2 – 60° with a step size of 0.02°. The interlayer distance was evaluated from the position of peak appearing at 2θ of ~10.5 – 11.5° using Bragg's law. The particle morphology was characterized using a Zeiss Supra 50 VP scanning electron microscope (SEM), usually at a potential of 5 kV. A Q50 thermogravimetric analyzer (TGA) was used to determine the degree of hydration in the synthesized materials by analyzing weight loss curves within the temperature range of 30 – 600 °C obtained under a heating rate of 10 °C·min⁻¹ in air. The surface area of the prepared materials was measured with surface area analyzer (NOVA 4200 e instrument) using multi point Brunauer Emmett and Teller (BET) method. Samples were degassed under vacuum overnight prior to measurement. Degas temperatures of 200°C and 250°C were used for the first and second measurements, respectively. Graphic representations of the BET data are provided in the Supporting Information (**Figure S7**).

The structures of LTO, NTO and KTO phases were determined via Rietveld refinement of the XRD patterns collected on a Rigaku SmartLab X-ray diffractometer with a 1760 W Cu K α X-ray source and a D/teX Ultra 1D detector. XRD patterns were collected with a step size of 0.05°, and a collection speed of 2°·min⁻¹. All Rietveld refinements were performed in GSAS-II.²⁹ The morphological and structural/chemical analysis of layered titanates was also made by bright-field transmission electron microscopy (TEM) imaging, annular dark field scanning TEM (ADF-STEM) imaging, selected area electron diffraction (SAED), high-resolution transmission electron microscopy (HRTEM), and Energy Dispersive X-Ray Spectroscopy (EDX) using a JEOL 2100F TEM/STEM operated at 200 kV. The elemental composition was measured using an EDX spectrometer (Oxford) equipped on the 2100F microscope.

2.3 Electrode fabrication

The electrodes were prepared by thoroughly mixing a 70:25:5 by weight mixture of active material (layered titanates), carbon black (conducting agent, Alfa Aesar) and poly(tetrafluoroethylene) (PTFE, binder, Sigma-Aldrich), respectively, in a rotary mixer (FlackTek™) at 2500 rpm. First, the active material and carbon black were dry-mixed over three 30-second mixing cycles. Then the PTFE with five drops of isopropanol were added and continued to be mixed for five 30-second cycles. Isopropanol was added to ensure proper wetting and a more uniform composition. The mixed slurry was poured carefully onto a glass slide and gently kneaded with a spatula and rolled by a test tube until a homogenous material of uniform consistency was obtained. This electrode film was then dried overnight in a conventional oven at 105 °C in air. Since the goal of this work is to establish synthesis – structure – properties relationships, and not to maximize the performance of layered titanates, no nanostructuring methods were applied to maximize the surface area of the active material particles. At the same time, all electrodes was prepared using the same protocol to enable reliable comparison of materials performance.

2.4 Electrochemical characterization

The electrochemical performance of the LTO, NTO and KTO electrodes was evaluated in aqueous 1 M Na₂SO₄ electrolyte in a 3-electrode Swagelok™ cell setup, where the working, counter and reference electrodes were the layered titanates, carbon (YP50) and Ag/AgCl, respectively. All electrochemical tests were carried out using a Biologic™ potentiostat. For initial analysis of electrochemical activity, cyclic voltammetry (CV) curves were obtained in a voltage window of -0.25 – 0.8 V at a scan rate of 1 mV s⁻¹. Once that had been ascertained, progressively higher scan rates of 2, 5 and 10 mV s⁻¹ were used to determine the performance of the electrodes towards faster voltage sweeps. The stability (cycling performance) of the electrodes were determined at a scan rate of 2 mV s⁻¹ over 100 cycles of operation.

3. Results and discussion

3.1 Structural, chemical and morphological characterization of single-phase layered titanates preintercalated with alkali ions

Figure 2(a) shows the XRD patterns of the synthesized materials. The XRD pattern of Na-preintercalated titanate resembles the one previously reported for the nonatitanate phase¹⁵, and corresponding Miller indexes are shown for the XRD pattern of NTO sample in **Figure 2(a)**. The overall appearance of the three XRD patterns is similar, implying the structural similarity of LTO, NTO and KTO samples. The presence of only a few pronounced reflections is typical for materials with lower levels of crystallinity as evidenced by the broad peaks. The interlayer distances were determined from the positions of the most intense peak that appears at $\sim 10.5 - 11.5^\circ 2\theta$ and found to be 8.25 Å in LTO, 7.95 Å in NTO and 7.75 Å in KTO layered phases. These results are in agreement with previously observed trends in the structure of chemically preintercalated bilayered vanadium oxides, where the interlayer distance was found to increase with the increase of the radius of hydrated interlayer ions²⁷.

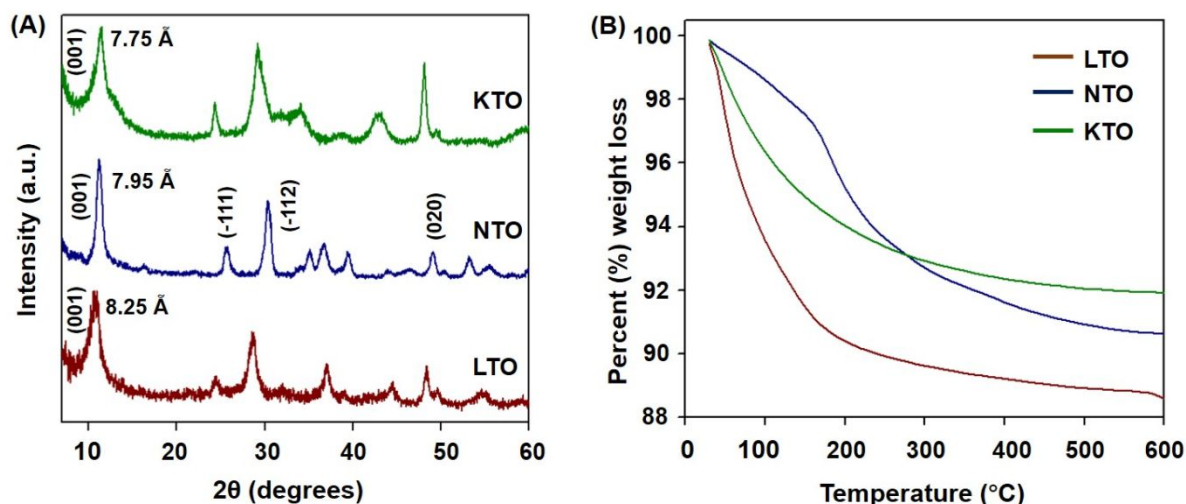


Figure 2. (a) XRD patterns and (b) TGA weight loss curves of the alkali ion preintercalated layered titanates, MTO (M = Li, Na, K).

Figure 2(b) demonstrates the characteristic TGA curves of the layered titanates. The weight loss, corresponding to different types of water, occurs in several steps. Initially, at temperatures up to 100 °C, the weight loss corresponds to the evaporation of surface water, followed by removal of the structural water from the interlayer region, between 100 – 600 °C. The degree of hydration, which has an important role in influencing the interlayer spacing and

electrochemical activity, is different in layered LTO, NTO and KTO materials under study. However, the accurate evaluation of the hydration degree requires the material unit formulas to be known and will be discussed in more detail below.

Figure 3 shows the SEM images of the LTO, NTO and KTO samples. **Figures 3 (a, d, g)** show the images obtained at low magnification allowing observation of particle agglomerates, whereas **Figures 3 (b, e, h)** show images obtained at a higher magnification clearly exhibiting morphology of the single particles. A considerable degree of variation in the bulk morphology is observed. The LTO particles (**Figure 3 (a, b)**) have a flower-like shape with individual two-dimensional (2D) plates or “peony-petal” like structures emanating from the center. The NTO (**Figure 3 (c, d)**) and KTO (**Figure 3 (e, f)**) samples crystallized as one-dimensional (1D) rod-like particles, however with subtle differences. The NTO particles exhibit uniform slender nanorod morphology with lengths of $\sim 1\text{-}2\ \mu\text{m}$ and the edge dimensions on the order of a few tens of nm. The KTO particles have similar 1D morphology, however they are thicker and stubbier, having lengths rarely exceeding $1\ \mu\text{m}$. High resolution SEM images indicate that particles of both NTO and KTO phases tend to grow together forming agglomerates of uniaxially aligned nanorods. In case of KTO, the tendency to agglomerate is more pronounced. Similar 1D rod-like morphology of sodium nonatitanates have been observed by Zhu *et al*³⁰. These results indicate that the variation of synthesis parameters (**Table 1**) strongly influences the morphology of layered titanates obtained via chemical preintercalation synthesis route.

Surface area analyses of the preintercalated layered titanate structures revealed KTO to have the greatest surface area, evincing a BET surface area of $150.4\ \text{m}^2/\text{g}$ and $146.1\ \text{m}^2/\text{g}$ following degas procedures at 200°C and 250°C , respectively; whereas, the LTO materials produced surface areas of $145.4\ \text{m}^2/\text{g}$ and $155.8\ \text{m}^2/\text{g}$, and the NTO analogue exhibited surface areas of $20.9\ \text{m}^2/\text{g}$ and $20.4\ \text{m}^2/\text{g}$ following degas procedures at the aforementioned temperatures, respectively. The dissimilar surface area of the NTO from the others aligns with prior dehydration studies, which describe the material losing water up to 600°C .¹⁵

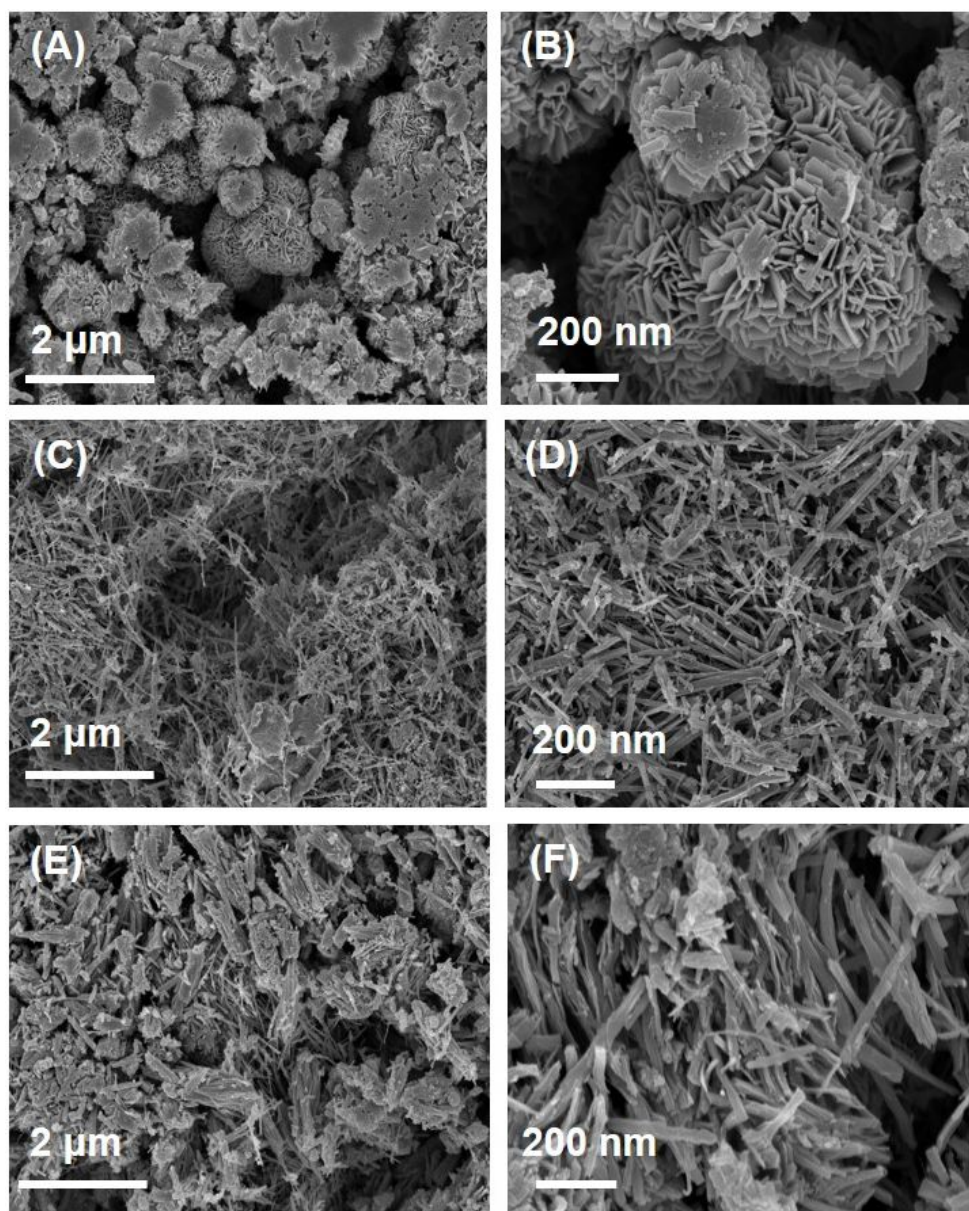


Figure 3. Morphology of layered alkali metal-ion preintercalated titanates: (a, b) LTO, (c, d) NTO, and (e, f) KTO. (a, c, e,) Low magnification and (b, d, e,) high magnification SEM images.

3.3 Electrochemical performance

The 1st, 50th and 100th cycles CV curves of the cells containing LTO, NTO and KTO working electrodes with 1 M Na₂SO₄ electrolyte at a scan rate of 2 mV s⁻¹ are shown in **Figure 4 (a-c)**. A voltage window of -0.25 to 0.80 V vs. Ag/AgCl reference electrode has been selected to accommodate a large enough voltage sweep window for the electrochemical activity to occur without the observation of signature increase in current due to the electrochemical water splitting phenomenon.

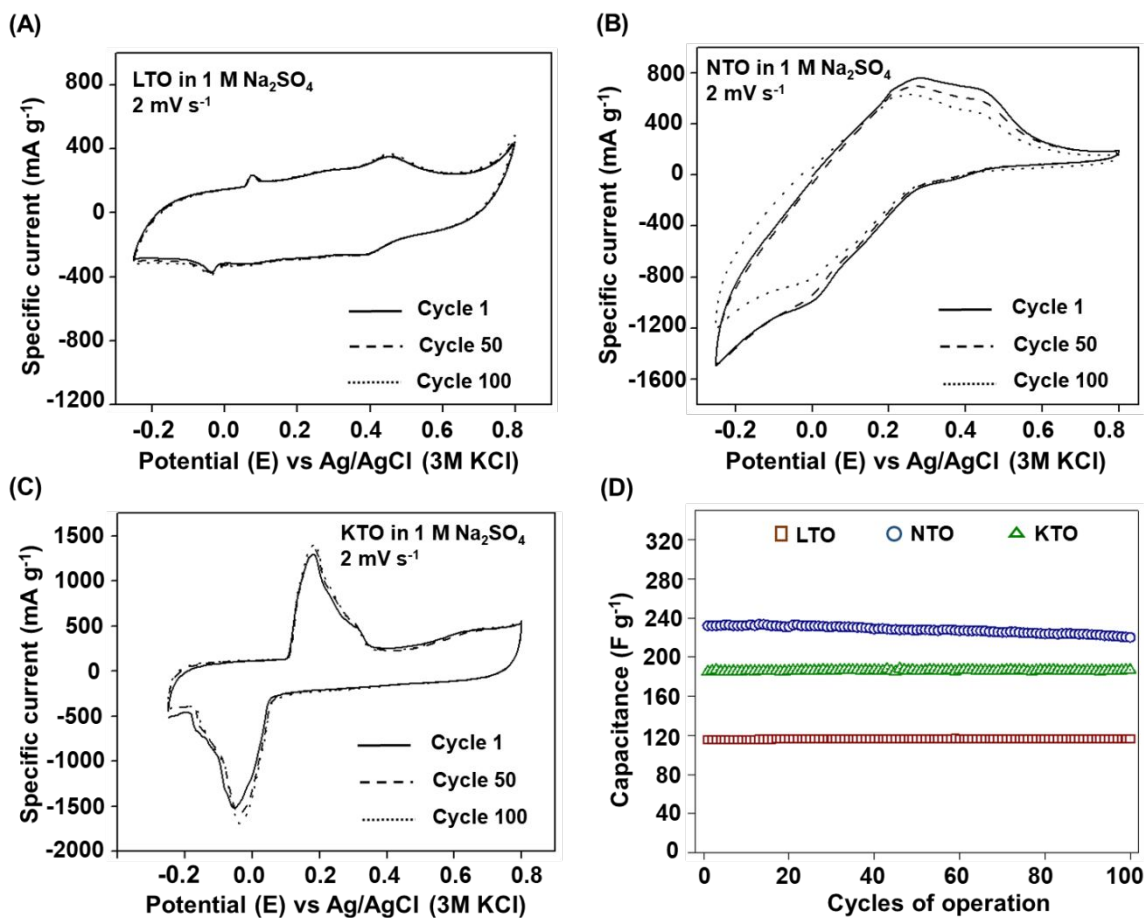


Figure 4. Electrochemical performance of alkali ion preintercalated layered titanates in aqueous cells with 1 M Na₂SO₄ electrolyte. (a – c) The 1st, 50th and 100th cycle CV curves of cells containing (a) LTO, (b) NTO, (c) KTO electrodes cycled at 2 mV s⁻¹. (d) Capacitance retention over 100 cycles of operation.

All three samples demonstrate considerable electrochemical activity, as indicated by the shape of CV curves. However, the shape of the CV curves is noticeably different. The cell with the LTO electrode exhibited a CV curve with an essentially rectangular shape and only two small pairs of peaks at ~ -0.05 - 0.10 V and ~ 0.4 - 0.5 V vs. Ag/AgCl (**Figure 4(a)**). On the other hand, the cell with the KTO electrode demonstrated a CV curve with a pair of distinct broad peaks at ~ -0.10 - 0.20 V vs. Ag/AgCl, each of which is likely to be a combination of several peaks (**Figure 4(c)**). The cell containing NTO electrode showed a CV curve with both large rectangular area and broad oxidation/reduction peaks. The differences in the shapes of CV curves imply that the charge storage mechanism in the synthesized layered titanates could depend on the nature of chemically preintercalated ion. The NTO electrode exhibits the highest capacitance at the scan rate of 2 mV

s^{-1} among the three layered titanates, delivering a maximum specific capacitance of 232.21 F g^{-1} . The KTO electrode demonstrates a lower capacitance of 184.88 F g^{-1} , and the LTO electrode exhibited the lowest capacitances of 115.38 F g^{-1} . **Figure 4 (d)** shows that the NTO electrode demonstrated a small amount of capacitance fading over 100 cycles, and was able to retain $\sim 95\%$ of the initial capacitance, whereas KTO and LTO electrodes showed no appreciable capacitance loss. The small capacitance loss can be attributed to the enhanced electrochemical activity of the NTO sample that could lead to more noticeable electrode degradation.

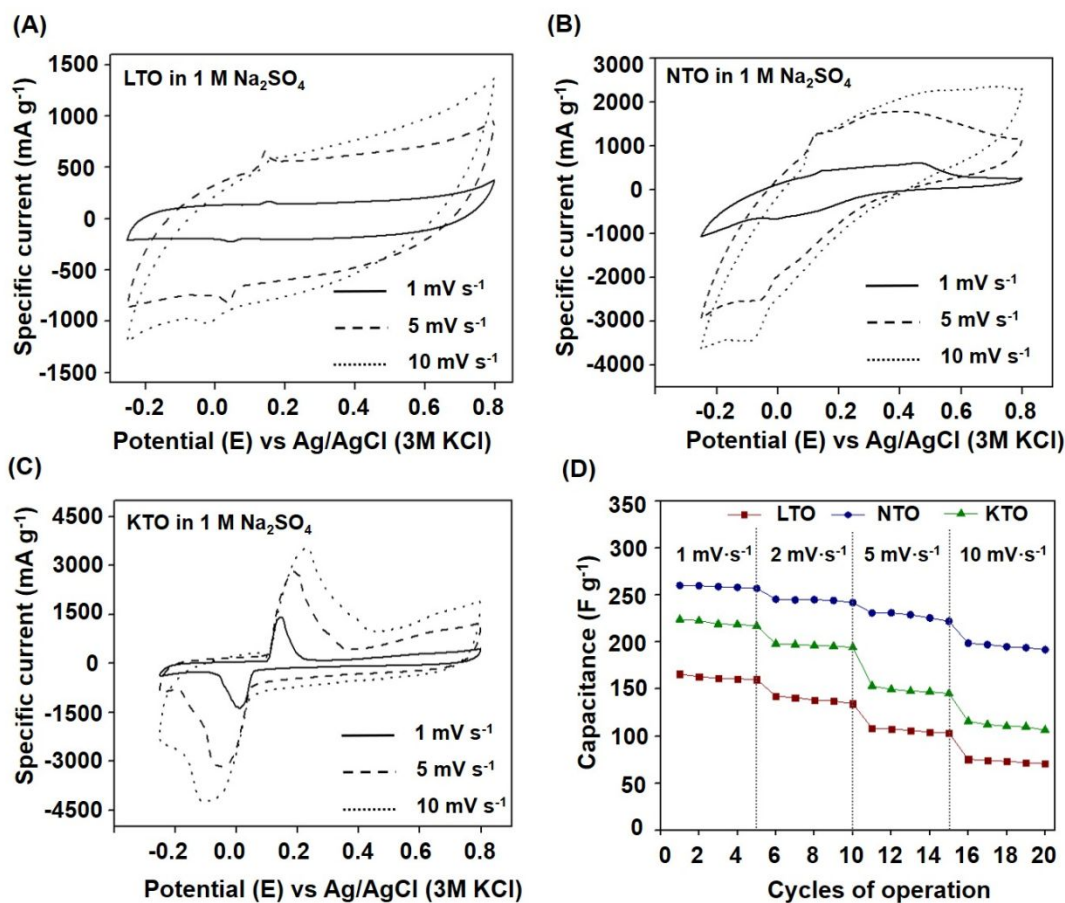


Figure 5. Rate performance of alkali ion preintercalated layered titanates in aqueous cells with 1 M Na₂SO₄ electrolyte. (a – c) CV curves of the cells containing (a) LTO, (b) NTO, (c) KTO electrodes at scan rates of 1, 5 and 10 $\text{mV}\cdot\text{s}^{-1}$. (d) Capacitance of LTO, NTO and KTO electrodes cycled for five cycles at increasing scan rates of 1, 2, 5 and 10 $\text{mV}\cdot\text{s}^{-1}$.

Figure 5 (a-c) demonstrates the CV curves of the cells containing LTO (**Figure 5(a)**), NTO (**Figure 5(b)**) and KTO (**Figure 5(c)**) electrodes at the scan rates of 1, 5 and 10 mV s^{-1} , and the values of capacitance are summarized in **Table 2**.

Table 2. Capacitance values of the cells containing LTO, NTO and KTO working electrodes with 1 M Na₂SO₄(aq.) electrolyte at the scan rates of 1, 5 and 10 mV·s⁻¹.

Working electrode	Capacitance (F·g ⁻¹) at 1 mV·s ⁻¹	Capacitance (F·g ⁻¹) at 5 mV·s ⁻¹	Capacitance (F·g ⁻¹) at 10 mV·s ⁻¹
LTO	166.03	108.20	75.29
NTO	260.23	230.92	198.75
KTO	224.08	153.21	115.69

At each of the gradually increasing scan rates, the trend in capacitance values is the same: NTO > KTO > LTO (**Figure 5** and **Table 2**). **Figure 5(d)** shows the rate performance of the LTO, NTO and KTO samples, plotted as capacitance value vs. cycle number at progressively increasing scan rates of 1, 2, 5 and 10 mV s⁻¹. The LTO, NTO and KTO electrodes demonstrated a capacitance decrease of 57.50 %, 26.28% and 52.49%, respectively, when the scan rate was changed from 1 to 10 mV·s⁻¹. The NTO electrode significantly outperforms both LTO and KTO electrodes with respect to its tolerance toward fast operating conditions.

Existing literature on layered transition metal oxides used as electrodes in energy storage systems has examples demonstrating that the electrochemical performance improves with the increase of the interlayer distance²⁶⁻²⁷. This trend was attributed to the larger volume of the interlayer region enabling facilitated diffusion of electrochemically cycled ions. However, in the case of the layered titanates studied in this work, it is observed that the trend in capacitance values is not directly proportional to the interlayer distance. Most notably, the LTO phase that exhibits the highest interlayer distance shows the lowest values of capacitance.

Two important factors that can shed light on the electrochemical performance of layered titanates are crystallinity and morphology of the materials. **Figure 3** shows that the NTO nanorods are well-dispersed, with only a small degree of agglomeration thus providing their entire surface area available for electrochemical charge storage. The KTO particles, on the other hand, are clumped/agglomerated which results in a loss of electrochemically active surface area. Furthermore, the LTO material crystallized as tightly intergrown flakes forming flower-like particles which also leads to the loss of surface area. Additionally, the broadening of the peaks and signal-to-noise ratio in the XRD patterns of the synthesized layered titanates (**Figure 2(a)**) suggest that the crystallinity of the materials decreases according to the following trend: NTO>KTO>LTO. However, the external morphology can only explain the electrochemical performance up to a point, as bulk morphology is only related to surface-based charge storage and does not play a crucial role

in intercalation type behavior, which is more dependent on the crystallographic structure. In fact, our BET measurements of the three layered titanates suggested the trend of surface area as $KTO \approx LTO > NTO$. The shape of CV curves shown in **Figure 4** and **5** indicated that the mechanism of charge storage was a combination of surface-based reactions and intercalation. A predominantly surface ion-absorption limited charge transfer process was noted in the LTO sample, while the defined CV peaks in KTO suggested a more diffusion-controlled intercalation charge storage process. Since layered titanates offer 2D interlayer regions for ion intercalation, the differences in morphology alone cannot satisfactorily explain the observed differences in electrochemical behavior of the three layered titanates. Therefore, the higher capacitances observed in NTO and KTO are more closely related to the crystallographic structure rather than the surface area. Also, as has been pointed out earlier, the layered titanates exhibit a great degree of structural polymorphism¹⁹⁻²⁰. Based on the similar overall appearance of the XRD patterns (**Figure 2(a)**), it was initially suggested that the synthesized layered titanates are isostructural. However, the considerable difference in the shape of the CV curves and variation in electrochemical performance led us to investigate the crystallographic structure of LTO, NTO and KTO phases in greater detail.

To understand the structural influence of intercalating different alkali metal cations into the layered titanate framework, numerous structural models were considered and evaluated by Rietveld refinement.

A Li_2TiO_3 model was developed for the LTO phase ($Cmmm$, $a=16.924 \text{ \AA}$, $b=3.7917 \text{ \AA}$, $c=3.0017 \text{ \AA}$, PDF #00-047-0123) shown in **Figure 6 (a, b)**, **Table 3**, and **Table S2**. The model accounts for all peaks suggesting that the phase has been accurately described and no impurities are present (**Figure 2a**). The structure is layered and characterized by repeating single layers of edge and corner sharing TiO_6 octahedra (**Figure 6(d)**). Water molecules and lithium ions reside in the large interlayer spaces. The material crystallizes in plate-like nanoparticles where the crystallites are thinnest along the layering axis (a).

The XRD pattern of the NTO phase fits well to a $\text{NaTi}_3\text{O}_6\text{OH}$ model ($C2/m$, $a=21.60 \text{ \AA}$, $b=3.7618 \text{ \AA}$, $c=11.96 \text{ \AA}$, $\beta=136.27^\circ$, PDF #01-080-7474) as shown in **Figure 6 (b, e)**, **Table 4**, and **Table S3** with all peaks accounted for and no impurities detected.³¹ $\text{NaTi}_3\text{O}_6\text{OH}$ is a different way to present a nonatitanate phase, where the unit formula of typically containing nine titanium atoms is divided by three. The structure consists of double layers of TiO_6 octahedra that are joined

by edge and corner linkages (**Figure 2(e)**). Sodium ions reside in the interlayer space where they are octahedrally coordinates to water molecules and oxygen atoms in the TiO_6 layers. The anisotropic peak broadening suggests that this $\text{NaTi}_3\text{O}_6\text{OH}$ materials possesses a needle-like morphology where the crystallites are significantly lengthened along the b axis.

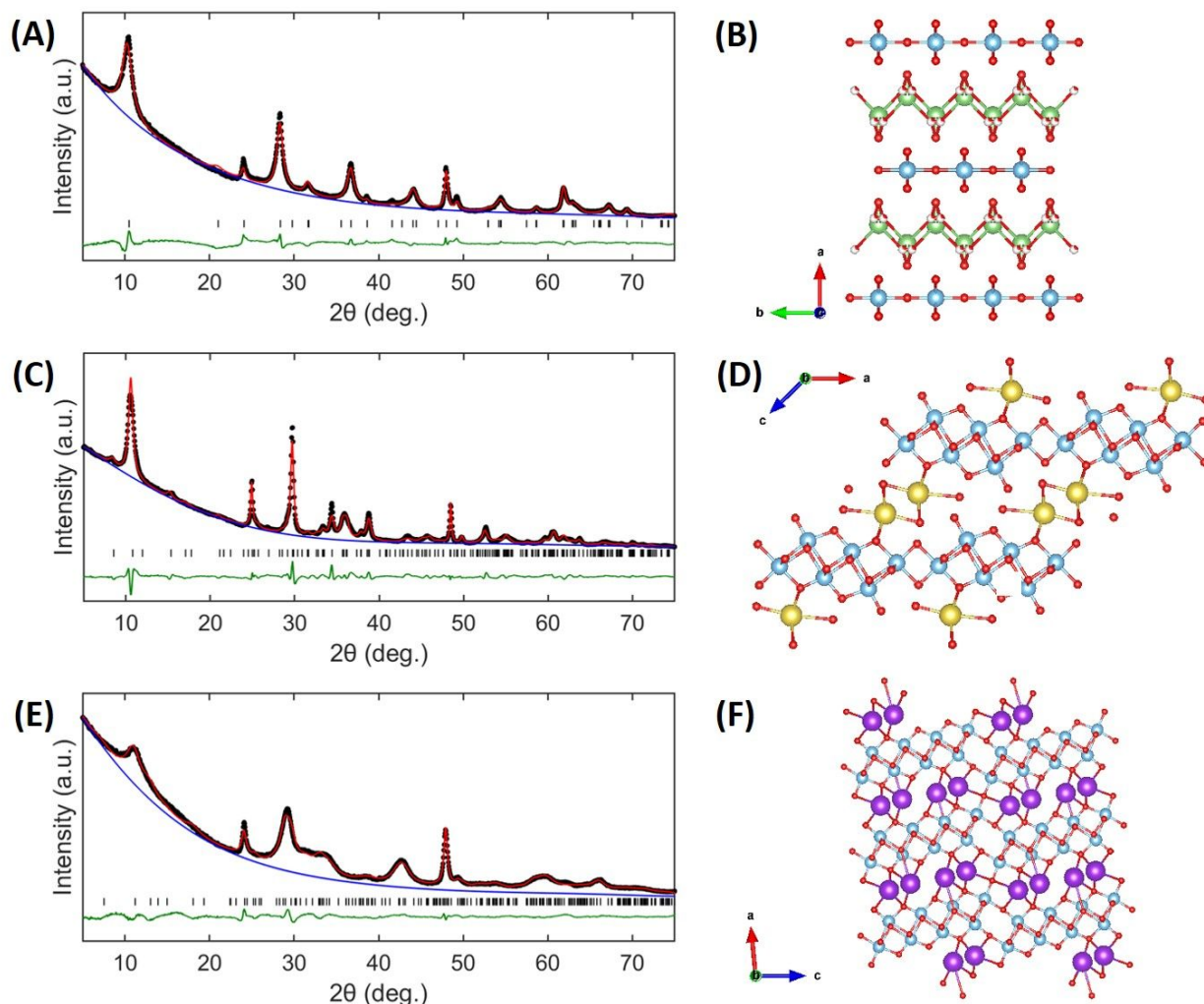


Figure 6. Analysis of the structure of alkali ion preintercalated layered titanates. (a, c, e) Rietveld refinements of X-ray diffraction patterns collected of (a) Li_2TiO_3 ($\%R_{\text{wp}}=4.13$), (c) $\text{NaTi}_3\text{O}_6\text{OH}$ ($\%R_{\text{wp}}=5.29$), and (e) $\text{K}_2\text{Ti}_8\text{O}_{17}$ ($\%R_{\text{wp}}=3.01$). The observed data is shown in black, the calculated data is red, the background is blue, and the difference between the observed and calculated data is shown in green. The black lines indicate the expected reflections from the models used. (b, d, f) Schematic illustrations of the crystal structures of (b) Li_2TiO_3 , (d) $\text{NaTi}_3\text{O}_6\text{OH}$, and (f) $\text{K}_2\text{Ti}_8\text{O}_{17}$. Titanium is light blue, oxygen is red, lithium is green, sodium is yellow, and potassium is purple.

The XRD pattern of the KTO phase fits well to a $K_2Ti_8O_{17}$ model with no impurities ($C2/m$, $a=15.96 \text{ \AA}$, $b=3.802 \text{ \AA}$, $c=11.93 \text{ \AA}$, $\beta=94.09^\circ$, PDF #01-080-2023) as shown in **Figure 6 (c, f)**, **Table 5**, and **Table S4**.³² $K_2Ti_8O_{17}$ is composed of edge and corner sharing double layers of TiO_6 octahedra with water and potassium ions in the interlayer region (**Figure 6(f)**). There are also oxide ions in the interlayer spaces that bridge one layer to the next; the potassium ions that are adjacent to these oxides are eight-coordinated while the other potassium ions are six-coordinated. The material possesses a needle-like morphology where the b axis is the dimension where crystallite lengthening is observed.

Table 3. Structural parameters obtained through Rietveld refinement of the X-ray diffraction pattern of Li_2TiO_3 .

	Value
Phase	Li_2TiO_3
Crystal System	Orthorhombic
Space Group	$Cmmm$
a (Å)	16.924(8)
b (Å)	3.7917(8)
c (Å)	3.0017(5)
β (°)	90
Interlayer Spacing (Å)	8.462(4)
Layering Axis	a
Crystallite size ((100), nm)	6.4(1)
Crystallite size ((011), nm)	27.2(8)

Table 4. Structural parameters obtained through Rietveld refinement of the X-ray diffraction pattern of $NaTi_3O_6OH$.

	Value
Phase	$NaTi_3O_6OH$
Crystal System	Monoclinic
Space Group	$C2/m$
a (Å)	21.60(8)
b (Å)	3.7618(3)
c (Å)	11.96(3)
β (°)	136.27(6)
Interlayer Spacing (Å)	8.27(2)
Layering Axis	c
Crystallite size ((010), nm)	64(3)
Crystallite size ((101), nm)	15.0(2)

Table 5 . Structural parameters obtained through Rietveld refinement of the X-ray diffraction pattern of $K_2Ti_8O_{17}$.

	Value
Phase	$K_2Ti_8O_{17}$
Crystal System	Monoclinic
Space Group	$C2/m$
<i>a</i> (Å)	15.96(2)
<i>b</i> (Å)	3.802(2)
<i>c</i> (Å)	11.93(1)
β (°)	94.09(9)
Interlayer Spacing (Å)	7.96(1)
Layering Axis	<i>a</i>
Crystallite size ((010), nm)	23.9(6)
Crystallite size ((101), nm)	4.6(1)

These results show that the general layered titanate framework can be preserved upon the introduction of Li^+ , Na^+ , and K^+ cations although some structural modification occur. The sodiated and potassiated materials are essentially isostructural, $C2/m$ and monoclinic crystal system, while the lithiated material is somewhat different, $Cmmm$ and orthorhombic. Similarly, the $K_2Ti_8O_{17}$ and $NaTi_3O_6OH$ adopt a needle-like morphology although the sodiated phase possesses significantly larger needles, while the Li_2TiO_3 adopts a more different plate-like morphology (**Tables 3-5**) in agreement with the SEM images (**Figure 3**).

Structural refinement revealed that the Ti-O layers in the structures of the NTO and KTO phases are built by double rows of Ti atoms bonded through oxygen atoms (called double layers below). On the contrary, the Ti-O layers in the LTO phase contain only single row of Ti atoms in octahedral coordination by oxygen atoms (called single layers below). The double layers are characterized by a larger number of redox centers that can reduce upon intercalation of the electrochemically cycled ions, compared to the single layers, which could contribute to higher values of capacitance that were experimentally observed for the NTO and KTO electrodes as compared to the LTO electrodes (**Figure 4** and **Figure 5**). When layered titanate phases with double Ti-O layers are compared to each other, the NTO phase exhibits both the larger interlayer spacing and higher values of capacitance at various scan rates, compared to the KTO phase, in agreement with the previously reported findings for the isostructural bilayered vanadium oxides²⁷.

Therefore, the observed electrochemical performance can be attributed to not only morphological features and crystallinity of the chemically preintercalated layered titanates, but also to the structure of Ti-O layers with $\text{Ti}^{4+/3+}$ redox centers that play a crucial role in capacitance contribution due to the bulk intercalation of electrochemically cycled ions. Further studies of layered phases that can be synthesized as polymorphs with single and double layers, such as $\alpha\text{-V}_2\text{O}_5$ (single layers) vs. $\delta\text{-V}_2\text{O}_5$ (double layers), are needed to better understand the role of the layer structure and the number of redox centers in the layer in energy storage.

Understanding of the structure and unit formulas of the three synthesized layered titanates allowed us to perform a more detailed analysis of the TGA weight loss curves (**Figure 2(b)**) with the aim to determine interlayer water content. The LTO, NTO and KTO samples lose $\sim 5\%$, $\sim 8\%$ and $\sim 4.5\%$ of their weights in the temperature range of $100 - 600^\circ\text{C}$, respectively. The temperature range was selected to exclude contributions from the evaporation of water molecules bound to the surface. The observed weight loss corresponds to the following hydration degrees: $\text{Li}_2\text{TiO}_3 \cdot 0.34\text{H}_2\text{O}$, $\text{NaTi}_3\text{O}_6\text{OH} \cdot 1.40\text{H}_2\text{O}$ and $\text{K}_2\text{Ti}_8\text{O}_{17}\text{OH} \cdot 1.96\text{H}_2\text{O}$. XRD analysis of the multiple batches of the synthesized LTO, NTO and KTO phases revealed that the interlayer distance slightly changes from batch to batch (**Figure S8** in the Supporting Information). This variation can be attributed to the different water content in the interlayer region, a parameter that is hard to accurately control experimentally. **Table S1** in the Supporting Information provides the variation of interlayer spacing, with the size of the hydrated preintercalated ion and hydration degrees.

To obtain additional information about the morphology and microstructure of Na- and K-preintercalated layered titanates, TEM/STEM images were collected using specimens supported on copper grids. As shown in **Figure 7(a)**, NTO exhibits a nanobelt morphology with lengths up to micrometers and an average diameter of 87.5 nm (see also **Figures S9(a, b)** and **Figure S10(a)** in the Supporting Information for more images taken from different areas and the corresponding statistic diameter distribution). SAED patterns were also taken from individual nanobelts, as illustrated in **Figure 7(b)** (from the marked area in **(a)** using dashed line circle), which can be indexed to the $(11\bar{1})$ and $(20\bar{1})$ planes of the monoclinic phase (S.G.: $C2/m$) with d spacings of 10.4 and 3.57 Å, respectively. From local studies using HRTEM (see one example in **Figure 7(c)** of a typical NTO nanobelt), we measured an interlayer spacing of 8.25 ± 0.08 Å (marked by the green dashed lines), which is in good agreement with the interlayer spacing along the c axis of 8.27 Å, as measured by the XRD results obtained from the same sample. The EDX maps (**Figure**

7(d)) demonstrate that Na, O, and Ti atoms are uniformly distributed in the NTO nanobelts without obvious aggregation.

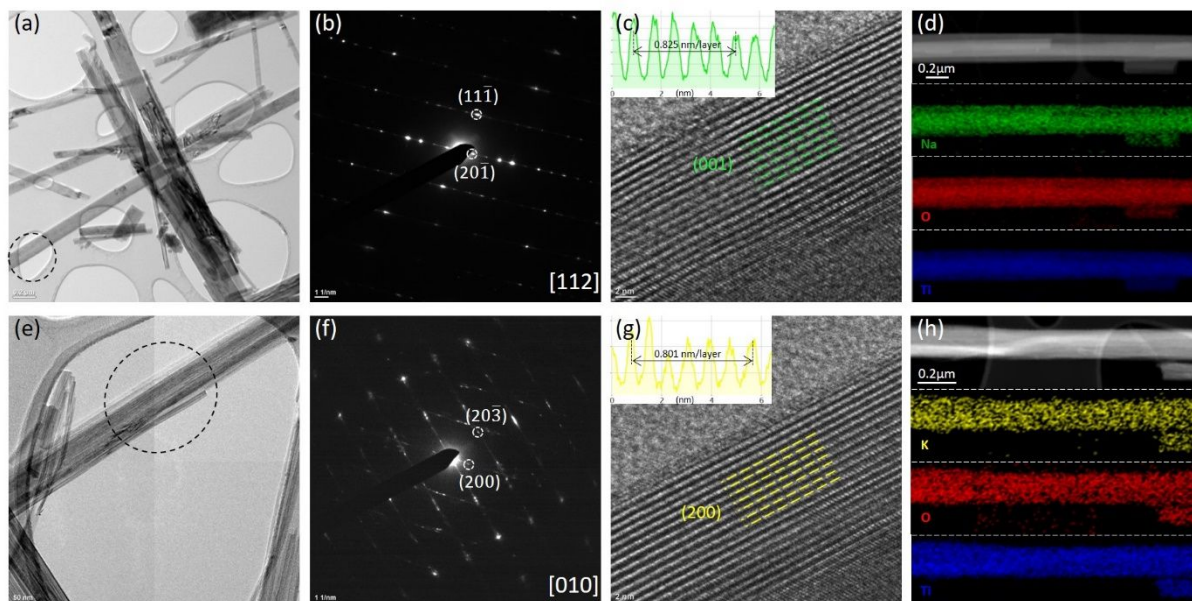


Figure 7. Microscopy observations of layered Na- and K-preintercalated titanates. (a) Bright-field transmission electron microscopy (TEM) imaging of $\text{NaTi}_3\text{O}_6\text{OH}\cdot n\text{H}_2\text{O}$, showing nanobelt shape with diameters ranging from 30 – 200 nm. (b) Selected area electron diffraction (SAED) pattern taken from the area marked in (a) using a dashed line circle. (c) High-resolution TEM (HRTEM) imaging of a single nanobelt with an interlayer spacing of 8.25 ± 0.08 Å, corresponding to the (001) facet of the monoclinic phase (S.G.: $C2/m$). Inset: intensity profile for calculating the interlayer spacing. (d) Elemental mapping of Na, O, and Ti atoms, in green, red, and blue, respectively. (e) Bright-field TEM imaging of $\text{K}_2\text{Ti}_8\text{O}_{17}\cdot n\text{H}_2\text{O}$, showing nanowire shape with diameters ranging from 3 – 20 nm. (f) SAED pattern taken from the area marked in (e) using a dashed line circle. (g) HRTEM image of a single nanowire with an interlayer spacing of 8.01 ± 0.09 Å, corresponding to the (200) facet of the monoclinic phase (S.G.: $C2/m$). Inset: intensity profile for calculating the interlayer spacing. (h) Elemental mapping of K, O, and Ti atoms, in yellow, red, and blue, respectively.

Similar studies were also made on the KTO sample, with the results presented in **Figures 7(e)-7(h)**. The sample mainly consists of nanowires of varying size, showing an average diameter of 9.5 nm based on 60 samples (**Figure 7(e)**; see also **Figures S9(c, d)** and **Figure S10(b)** in the Supporting Information for more images taken from different areas and the corresponding statistic diameter distribution), much smaller than those of NTO material (**Figure 7(a)**). Similarly, the lengths of nanowires can reach several microns and the fine nanowires prefer to bunch together. From the SAED pattern (**Figure 7(f)**); from the marked bunch of nanowires shown in **Figure 7(e)**,

the sample exhibits a polycrystalline nature, consistent with the XRD patterns showing feature patterns indexed to the (200) and (20 $\bar{3}$) planes. The interlayer spacing along the a axis is around 8.01 ± 0.09 Å according to the HRTEM (**Figure 7(g)**), which is in a good agreement with the structure refinement results shown in **Table 5**. EDX maps (**Figure 7(h)**) reveal the homogeneous distribution of different elements (K, O, and Ti) in the KTO nanowires.

Alkali ion preintercalated layered titanates synthesized in this work served as a model material system to establish correlations between the crystal structure and electrochemical performance in an aqueous energy storage system. The electrode fabrication process has not been optimized. Further improvements can be achieved by applying nanostructuring strategies. Additionally, low-concentration aqueous electrolytes have been used in this work. The advent of water-in-salt electrolyte systems opens opportunities to obtain substantially higher performance parameters shown by layered titanates. Our finding that double layers can exhibit substantially higher electrochemical activity than single layers is important for future design and synthesis of 2D heterostructure electrodes built by alternating redox active oxide layers and electronically conductive layers³³. Understanding of the redox activity of differently structured layers is crucial in selecting the most promising candidates for 2D heterostructure fabrication through exfoliation/reassembly approach. Our results indicate that in case of alkali ion preintercalated layered titanates, the NTO phase with nonatitanate structure has the highest potential to lead to high performance when integrated in 2D heterostructure architecture with conducting layers, such as graphene-like materials.

4. Conclusion

In conclusion, we report the successful preparation of alkali metal ion pre-intercalated layered ternary titanates using a novel scalable synthesis method that consist in a sol-gel step followed by a hydrothermal treatment step, both performed in a basic aqueous environment. The synthesis process parameters were found for each material to ensure the pure layered phase formation. Structural characterization results confirm formation of the layered phases; however, SEM imaging shows distinct morphological variations. The NTO and KTO samples exhibit 1D nanorod like morphology, with the KTO rods being shorter and more aggregated, whereas the LTO exhibits intergrown nanoplatelet morphology. The BET measurements suggest the trend of surface area as $KTO \approx LTO > NTO$. The interlayer spacing increases with larger sized preintercalated

ions, with KTO phase exhibiting the smallest interlayer spacing of 7.75 Å and LTO phase showing the largest interlayer spacing of 8.25 Å. Analysis of the MTO (M = Li, Na, K) materials as electrodes in cells with aqueous neutral electrolyte demonstrates the superior capacitance delivered by the NTO electrode (260.23 F g⁻¹), followed by the KTO electrode (224.47 F g⁻¹) and then the LTO electrode (166.03 F g⁻¹) at a scan rate of 1 mV·s⁻¹. The obtained capacitance values have been attributed to a combination of factors, including different morphologies of the layered titanate particles, interlayer distance, and the number of Ti⁴⁺/Ti³⁺ redox centers in Ti-O layers. The observed trend of electrochemical performance is repeated at higher scan rates, with the NTO sample exhibiting capacitance loss of 26.28 % when the scan rate was changed from 1 to 10 mV·s⁻¹, whereas the capacitance decrease under the same electrochemical testing conditions in case of the KTO and LTO electrodes were 52.49 % and 57.50 %, respectively. To the best of our knowledge, this report is the first systematic study that deals comprehensively with the synthesis of varying alkali ion preintercalated layered titanates and their electrochemistry in aqueous energy storage systems.

SUPPORTING INFORMATION

Images of step-by-step synthesis of NTO, KTO and LTO. XRD patterns of LTO, NTO and KTO samples synthesized by non-optimal and optimal techniques. Table of hydration degrees, interlayer spacing and size of hydrated ionic radii. Graphic representation of BET measurements. TEM images of NTO and KTO nanorods. Table showing Rietveld refinement parameters and atomic positions.

Acknowledgements

The authors acknowledge the Center for Mesoscale Transport Properties, an Energy Frontier Research Center supported by the U.S. Department of Energy, Office of Science, Basic Energy Sciences, under Award No. DE-SC0012673 for financial support. This research used resources of the Center for Functional Nanomaterials, which is a U.S. DOE Office of Science Facility, at Brookhaven National Laboratory under Contract No. DE-SC0012704. CAS acknowledges support from the NIH Institutional Research and Academic Career Development Award and New York Consortium for the Advancement of Postdoctoral Scholars (IRACDA-NYCAPS), award

K12-GM102778. EST acknowledges support as the William and Jane Knapp Chair in Energy and the Environment.

Author Contributions

E.P. and S.M. developed the concept and designed the experiments. S.M. carried out the experimental work including synthesis, characterization and electrochemical testing. C.D.Q., A.M., E.T and K.T. performed structure refinement. C.S. performed BET data collection under the guidance of L.W and A.M. S.Y. carried out TEM/STEM analysis under the supervision of F.W. All authors contributed to the analysis and interpretation of obtained experimental data and writing of the manuscript.

References:

1. Kim, D.; Kang, S.-H.; Slater, M.; Rood, S.; Vaughey, J. T.; Karan, N.; Balasubramanian, M.; Johnson, C. S., Enabling Sodium Batteries Using Lithium-Substituted Sodium Layered Transition Metal Oxide Cathodes. *Advanced Energy Materials* **2011**, *1* (3), 333-336.
2. Rogelj, J.; Schaeffer, M.; Meinshausen, M.; Knutti, R.; Alcamo, J.; Riahi, K.; Hare, W., Zero emission targets as long-term global goals for climate protection. *Environmental Research Letters* **2015**, *10* (10), 105007.
3. Kim, H.; Kim, H.; Ding, Z.; Lee, M. H.; Lim, K.; Yoon, G.; Kang, K., Recent Progress in Electrode Materials for Sodium-Ion Batteries. *Advanced Energy Materials* **2016**, *6*, 1600943.
4. Kim, S. W.; Seo, D. H.; Ma, X.; Ceder, G.; Kang, K., Electrode materials for rechargeable sodium-ion batteries: potential alternatives to current lithium-ion batteries. *Advanced Energy Materials* **2012**, *2*, 710-721.
5. Yan, J.; Wang, J.; Liu, H.; Bakenov, Z.; Gosselink, D.; Chen, P., Rechargeable hybrid aqueous batteries. *Journal of Power Sources* **2012**, *216*, 222-226.
6. Slater, M. D.; Kim, D.; Lee, E.; Johnson, C. S., Sodium-Ion Batteries. *Advanced Functional Materials* **2013**, *23* (8), 947-958.
7. Kim, K.-T.; Ali, G.; Chung, K. Y.; Yoon, C. S.; Yashiro, H.; Sun, Y.-K.; Lu, J.; Amine, K.; Myung, S.-T., Anatase Titania Nanorods as an Intercalation Anode Material for Rechargeable Sodium Batteries. *Nano Letters* **2014**, *14* (2), 416-422.
8. Lee, S.; Ha, J.; Choi, J.; Song, T.; Lee, J. W.; Paik, U., 3D Cross-Linked Nanoweb Architecture of Binder-Free TiO₂ Electrodes for Lithium Ion Batteries. *ACS Applied Materials & Interfaces* **2013**, *5* (22), 11525-11529.
9. Guo, S.; Yi, J.; Sun, Y.; Zhou, H., Recent advances in titanium-based electrode materials for stationary sodium-ion batteries. *Energy & Environmental Science* **2016**, *9* (10), 2978-3006.
10. Reyes-Coronado, D.; Rodríguez-Gattorno, G.; Espinosa-Pesqueira, M. E.; Cab, C.; de Coss, R.; Oskam, G., Phase-pure TiO₂ nanoparticles: anatase, brookite and rutile. *Nanotechnology* **2008**, *19* (14), 145605.
11. Mukherjee, S.; Singh, G., Two-Dimensional Anode Materials for Non-lithium Metal-Ion Batteries. *ACS Applied Energy Materials* **2019**, *2* (2), 932-955.
12. Pomerantseva, E.; Resini, C.; Kovnir, K.; Kolen'ko, Y. V., Emerging nanostructured electrode materials for water electrolysis and rechargeable beyond Li-ion batteries. *Advances in Physics: X* **2017**, *2* (2), 211-253.
13. Li, N.; Zhang, L.; Chen, Y.; Fang, M.; Zhang, J.; Wang, H., Highly Efficient, Irreversible and Selective Ion Exchange Property of Layered Titanate Nanostructures. *Advanced Functional Materials* **2012**, *22* (4), 835-841.
14. Xie, J.; Wang, X.; Zhou, Y., Understanding Formation Mechanism of Titanate Nanowires through Hydrothermal Treatment of Various Ti-Containing Precursors in Basic Solutions. *Journal of Materials Science & Technology* **2012**, *28* (6), 488-494.
15. Shirpour, M.; Cabana, J.; Doeff, M., New materials based on a layered sodium titanate for dual electrochemical Na and Li intercalation systems. *Energy & Environmental Science* **2013**, *6* (8), 2538-2547.
16. Shirpour, M.; Cabana, J.; Doeff, M., Lepidocrocite-type Layered Titanate Structures: New Lithium and Sodium Ion Intercalation Anode Materials. *Chemistry of Materials* **2014**, *26*, 2502-2512.
17. Yates, S. F.; Sylvester, P., Sodium nonatitanate: a highly selective inorganic ion exchanger for strontium. *Separation Science and Technology* **2001**, *36* (5-6), 867-883.
18. Watanabe, M.; Bando, Y.; Tsutsumi, M., A new member of sodium titanates, Na₂Ti₉O₁₉. *Journal of Solid State Chemistry* **1979**, *28* (3), 397-399.
19. Sasaki, T.; Kooli, F.; Iida, M.; Michiue, Y.; Takenouchi, S.; Yajima, Y.; Izumi, F.; Chakoumakos, B. C.; Watanabe, M., A Mixed Alkali Metal Titanate with the Lepidocrocite-like Layered Structure. Preparation, Crystal Structure, Protonic Form, and Acid-Base Intercalation Properties. *Chemistry of Materials* **1998**, *10* (12), 4123-4128.

20. Huang, J.; Cao, Y.; Deng, Z.; Tong, H., Formation of titanate nanostructures under different NaOH concentration and their application in wastewater treatment. *Journal of Solid State Chemistry* **2011**, *184*, 712-719.
21. Dong, Y.; Wu, Z.-S.; Zheng, S.; Wang, X.; Qin, J.; Wang, S.; Shi, X.; Bao, X., Ti₃C₂ MXene-Derived Sodium/Potassium Titanate Nanoribbons for High-Performance Sodium/Potassium Ion Batteries with Enhanced Capacities. *ACS Nano* **2017**, *11* (5), 4792-4800.
22. Yin, J.; Qi, L.; Wang, H., Sodium Titanate Nanotubes as Negative Electrode Materials for Sodium-Ion Capacitors. *ACS Applied Materials & Interfaces* **2012**, *4* (5), 2762-2768.
23. Doeff, M. M.; Cabana, J.; Shirpour, M., Titanate Anodes for Sodium Ion Batteries. *Journal of Inorganic and Organometallic Polymers and Materials* **2014**, *24* (1), 5-14.
24. Fleischmann, S.; Sun, Y.; Osti, N. C.; Wang, R.; Mamontov, E.; Jiang, D.-e.; Augustyn, V., Interlayer separation in hydrogen titanates enables electrochemical proton intercalation. *Journal of Materials Chemistry A* **2020**, *8* (1), 412-421.
25. Mao, Y.; Kanungo, M.; Hemraj-Benny, T.; Wong, S. S., Synthesis and Growth Mechanism of Titanate and Titania One-Dimensional Nanostructures Self-Assembled into Hollow Micrometer-Scale Spherical Aggregates. *Journal of Physical Chemistry B* **2006**, *110*, 702-710.
26. Clites, M.; Byles, B. W.; Pomerantseva, E., Effect of aging and hydrothermal treatment on electrochemical performance of chemically pre-intercalated Na-V-O nanowires for Na-ion batteries. *Journal of Materials Chemistry A* **2016**, *4* (20), 7754-7761.
27. Clites, M.; Pomerantseva, E., Bilayered vanadium oxides by chemical pre-intercalation of alkali and alkali-earth ions as battery electrodes. *Energy Storage Materials* **2018**, *11*, 30-37.
28. Kunxu, Z.; Gao, H.; Guoxin, h.; Liu, M.; Wang, H., Scalable synthesis of hierarchical hollow Li₄Ti₅O₁₂ microspheres assembled by zigzag-like nanosheets for high rate lithium-ion batteries. *Journal of Power Sources* **2017**, *340*, 263-272.
29. Toby, B. H.; Von Dreele, R. B., GSAS-II: the genesis of a modern open-source all purpose crystallography software package. *J. Appl. Crystallogr.* **2013**, *46* (2), 544-549.
30. Zhang, H.; Gao, X. P.; Li, G. R.; Yan, T. Y.; Zhu, H. Y., Electrochemical lithium storage of sodium titanate nanotubes and nanorods. *Electrochimica Acta* **2008**, *53* (24), 7061-7068.
31. Andrusenko, I.; Mugnaioli, E.; Gorelik, T. E.; Koll, D.; Panthoefer, M.; Tremel, W.; Kolb, U., Structure analysis of titanate nanorods by automated electron diffraction tomography. *Acta Crystallogr., Sect. B: Struct. Sci.* **2011**, *67* (3), 218-225.
32. Sasaki, T.; Watanabe, M.; Fujiki, Y.; Kitami, Y.; Yokoyama, M., Crystal structure of octatitanate M₂Ti₈O₁₇ (M = potassium, rubidium). *J. Solid State Chem.* **1991**, *92* (2), 537-42.
33. Pomerantseva, E.; Gogotsi, Y., Two-dimensional heterostructures for energy storage. *Nature Energy* **2017**, *2* (7), 17089.